J Solid State Electrochem (2015) 19:697–702
DOI 10.1007/s10008-014-2654-1

ORIGINAL PAPER

High performance all-solid-state lithium/sulfur batteries using lithium argyrodite electrolyte

Maohua Chen · Stefan Adams

Received: 14 July 2014 / Revised: 30 September 2014 / Accepted: 4 October 2014 / Published online: 17 October 2014

Abstract Among the known fast Li^+ ion conducting solids, thiophosphates and especially lithium argyrodites Li_6PS_5X (X= Cl, Br) exhibit a great potential due to their high ionic conductivities and electrochemical stability. Here, we prepare all-solid-state lithium secondary batteries combining sulfur as the active cathode material with argyrodite-type Li_6PS_5Br as the solid electrolyte. Composite cathode powder of sulfur, Li_6PS_5Br and super P carbon are fabricated by a two-step ball milling at high rotating speed of 500 rpm, yielding a uniform composite cathode mixture with a particle size smaller than 100 nm. The resulting all-solid-state S/Li_6PS_5Br/In-Li batteries with S contents varied over the range of 20–40 wt% show a maximum capacity of 1460 mAh/g (with respect to the weight of sulfur) and a reversible capacity of up to 1080 mAh/g after 50 cycles at C/10 rate. Ex situ X-ray diffraction (XRD) results demonstrate that Li_6PS_5Br undergoes no structural change throughout the cycling.

Keywords All-solid-state batteries · Lithium argyrodite · Solid electrolytes · Sulfur cathodes · High-energy ball milling · Lithium/sulfur cells

Introduction

The aim to achieve a transition to a more sustainable transport system based on electric vehicles and the constantly growing need for portable electronic devices lead to a strong demand for safe, affordable, high energy density storage systems. The high theoretical specific capacity (1672 mAh/g) and energy density (2567 Wh/kg), low cost, and low toxicity of lithium/sulfur (Li/S) batteries have turned these batteries into one of the most promising contenders to overcome the energy density limitations of lithium-ion batteries [1]. However, there are still a number of challenges to be addressed in order to realize the full potential of Li/S batteries in commercially viable devices. For example, lithium polysulfides formed intermediately during the discharge of sulfur are highly soluble in conventional organic liquid electrolytes, which lead to fast capacity fading of liquid electrolyte Li/S batteries during cycling. Besides exploring more compatible liquid electrolytes [2] or suitable additives [3], using solid electrolytes that are impermeable to polysulfides in place of liquid electrolytes appears to be a promising strategy to eliminate this issue. Kobayashi et al. [4] reported all-solid-state Li/S batteries using thio-LISICON as an electrolyte, while Nagao et al. [5, 6] and Agostini et al. [7] used glass-ceramic and glassy Li_2S-P_2S_5 solid electrolytes, respectively. Lin et al. [8] prepared all-solid-state batteries using Li_3PS_4 solid electrolyte and polysulfidophosphate cathodes. The polysulfidophosphates were prepared by reacting sulfur with Li_3PS_4 in solution, in order to improve the ionic conductivity of sulfur. Here, we focus on lithium argyrodite Li_6PS_5Br solid electrolyte [9, 10], which combines high ionic conductivity (~10^{-3} S/cm) with suitable electrochemical stability [11–13]. The first reported argyrodite-based all-solid-state batteries employed $Li_4Ti_5O_{12}$ (LTO) as a zero-expansion insertion electrode material in combination with Li_6PS_5Br electrolyte [14]. Later, a LTO:Li_6PS_5Cl:Li battery showed significantly enhanced room temperature cycling performance [12]. Recently, we prepared all-solid-state batteries combining Li_6PS_5Br as the electrolyte with the high capacity conversion cathode materials CuS (reaching an initial capacity of 650 mAh/g) or Cu-Li_2S (with

M. Chen · S. Adams
Department of Materials Science and Engineering, National University of Singapore, 9 Engineering Drive 1, Singapore 117576, Singapore

S. Adams (✉)
Department of Materials Science and Engineering, National University of Singapore, 5 Engineering Drive 2, E2 #05-22, Singapore 117579, Singapore
e-mail: mseasn@nus.edu.sg

an initial capacity of 445 mAh/g) [13, 15]. It was however found that Cu^+ partially substitute Li^+ in both the solid electrolyte and the active materials during cycling, leading to the reversible formation of mixed mobile ion products of $Cu_xLi_{6-x}PS_5Br$ and $Cu_yLi_{2-y}S$.

In this study, we report a detailed study on the first all-solid-state S/Li_6PS_5Br/In-Li batteries, exploring their cycling performance, the stability of the solid electrolyte, and the aging mechanism. The studied lithium/sulfur cells showed a maximum discharge capacity of 1460 mAh/g (for 25 wt% S). A cell with 20 wt% S presented an initial discharge capacity of 1355 mAh/g and retained a reversible capacity of 1080 mAh/g after 50 cycles at the rate of C/10.

Experimental

Li_6PS_5Br was fabricated by ball milling and subsequent heat treatment. Details of the synthesis can be found in our earlier work [13]. In brief, a stoichiometric mixture of Li_2S, P_2S_5, and LiBr was milled at a rotating speed of 500 rpm for 10 h in a 45-ml zirconia bowl using a high-energy planetary ball mill (Fritsch Pulverisette 7). The ball-milled precursor mixture was pelletized and annealed at 300 °C for 5 h.

In order to prepare the sulfur composite cathode, sulfur, and super P carbon were mixed with a weight ratio of 2:1 and ball milled at 500 rpm for 5 h at room temperature. Thereafter, Li_6PS_5Br was added to this mixture, leading to a total weight ratio of S:Li_6PS_5Br:C=p:(100–1.5 p):0.5p with p=20, 25, 30, or 40. The resulting mixtures were further ball milled at 500 rpm for 30 min to ensure a thorough mixing. The ball milling was performed in a 45-ml zirconia bowl using a balls-to-powder weight ratio of 15:1. The entire preparation procedure was conducted under argon gas atmosphere. X-ray diffraction (XRD) measurement was conducted on both the pristine sulfur and ball-milled sulfur-carbon composite with a Bruker D8 Advance diffractometer (using Cu K_α radiation). The morphologies of the pristine sulfur, pristine carbon, ball-milled sulfur-carbon composite, and composite cathode powder were characterized by scanning electron microscopy (SEM, Zeiss Supra 40 VP). The homogeneity of the distribution of Li_6PS_5Br within the sulfur composite cathode powder was investigated by immersing a composite cathode powder sample in deionized (DI) water so that the Li_6PS_5Br was dissolved, leaving only the insoluble sulfur-carbon components of the composite, which after drying at room temperature was investigated by SEM.

For the assembly of all-solid-state S/Li_6PS_5Br/In-Li cells, 100 mg of Li_6PS_5Br solid electrolyte powder and 7.5–15 mg of composite cathode powder (keeping the amount of sulfur constant at 3 mg) were pelletized in a 13-mm die under a pressure of 6000 kg/cm^2. This yields cells with a cathode layer thickness of 30–40 μm and a solid electrolyte layer thickness of around 300 μm. An indium-lithium foil as anode was placed on the electrolyte side of the pellet, and the stack was sealed in a 13-mm Swagelok cell. The complete cell assembly process was carried out under argon atmosphere.

Cyclic voltammetry was performed on the all-solid-state S/Li_6PS_5Br/In-Li cells in the voltage range of 0.4 to 2.4 V vs. In-Li (which corresponds to 1.0 to 3.0 V vs. Li/Li^+) at a scanning rate of 0.02 mV/s using a potentiostat/galvonostat (Arbin BT2000). Room temperature cyclic performance of the S/Li_6PS_5Br/In-Li cell was investigated at the rate of C/10, i.e., a current density of 167 mA per gram of sulfur, between 0.4 and 2.4 V vs. In-Li (1.0–3.0 V vs. Li/Li^+). XRD investigations of the composite cathode before cycling and after 101 cycles (discharged state) were undertaken to explore possible structural variations such as those found in our previous studies using Cu-Li_2S electrodes [13]. During the XRD measurement, the composite cathodes were protected using Mylar film to avoid any reaction with air.

Results and discussion

XRD patterns of the pristine sulfur and ball-milled sulfur-carbon composite are shown in Fig. 1. For the pristine sulfur, all the diffraction peaks could be readily indexed to the orthorhombic phase of α-S. During high-speed ball milling with carbon, sulfur melts and resolidifies as an amorphous phase, leaving only some broad peaks attributed to the carbon in the XRD pattern of the S/C composite. According to Ji et al. [16] and Nagao et al. [5], this amorphization of sulfur increases the practical specific capacity of sulfur cathodes in both conventional liquid electrolyte and all-solid-state lithium batteries. This may be tentatively attributed to the intimate contact of S with the carbon and/or the introduction of more defect energy during ball milling. It can also not be excluded that sulfur reacts with functional groups on the surface of super P carbon

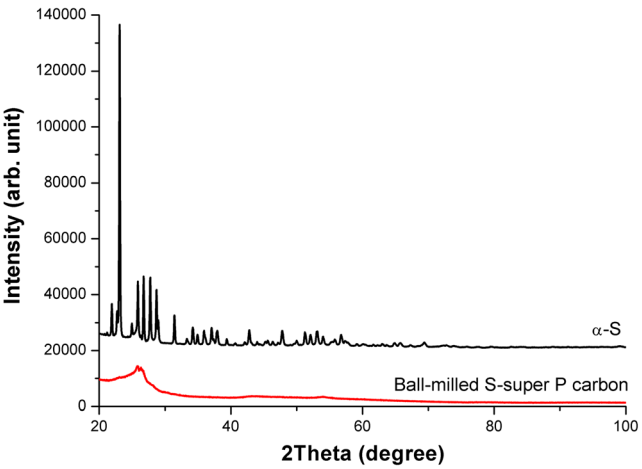

Fig. 1 XRD patterns of pristine sulfur and ball-milled sulfur-carbon composite

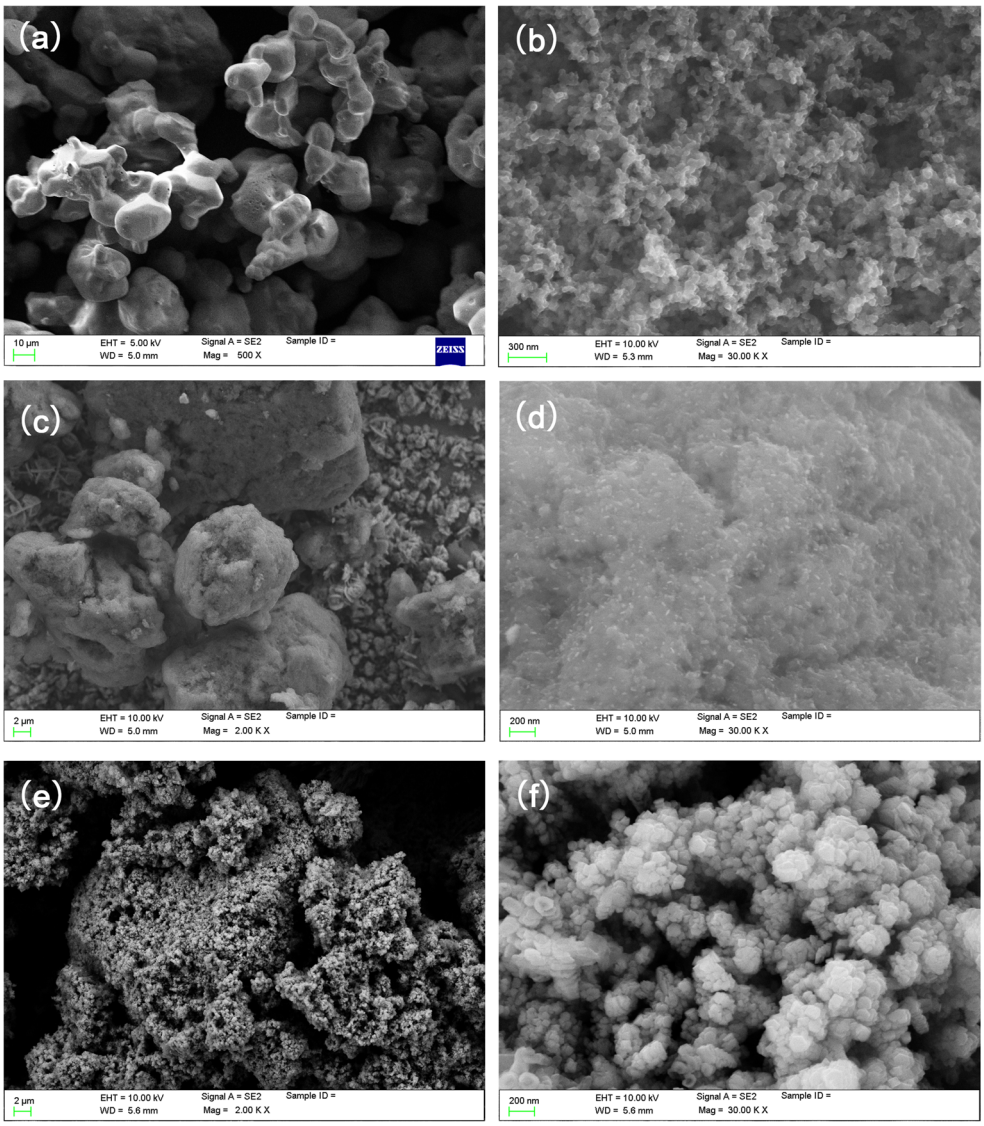

Fig. 2 SEM images of **a** pristine sulfur, **b** pristine super P carbon, **c**, **d** ball-milled sulfur-carbon composite, and **e**, **f** sulfur composite cathode powder (containing 20 wt% S) after removing Li_6PS_5Br

analogous to the "inverse vulcanization" discussed by Simmonds et al. [17]. While Nagao et al. realized the amorphization of sulfur by ball milling twice [5] or by high-temperature ball milling [6], we achieved the complete amorphization of sulfur in the first ball milling step at room temperature by choosing a higher ball milling speed of 500 rpm instead of 370 rpm. Consequently, the second ball milling step after adding the solid electrolyte serves only the purpose of ensuring a homogeneous mixing of the composite cathode and thus could be substantially reduced to 30 min (compared to 5 h employed by Nagao et al.). In our case of using a crystalline thiophosphate solid electrolyte, this is important as it minimizes structural damage to the argyrodite phase from ball milling and an amorphous phase of the same condition would have a nearly two orders of magnitude lower conductivity.

The microstructure of the pristine sulfur, super P carbon, ball-milled sulfur-carbon composite, and composite cathode powder after dissolving Li_6PS_5Br was investigated using SEM, as shown in Fig. 2. Pristine sulfur contained particles larger than 10 μm in size (see Fig. 2a), while the particle size of the pristine carbon (see Fig. 2b) was smaller than 100 nm. After the first ball milling, sulfur and carbon were uniformly mixed (denoted as 1st S-C), forming dense micrometer-sized particles, as shown in Fig. 2c, d. As a result of the low melting point of sulfur and the high ball milling speed (500 rpm), sulfur melts during high-energy ball milling. The molten sulfur then fills the pores in the carbon phase and surrounds the carbon, forming dense mesoscale particles.

To study the distribution of solid electrolyte within the composite cathode powder (after the second ball milling) by SEM, Li_6PS_5Br was removed by immersing the powder in DI water, leaving only the sulfur-carbon composite (denoted as 2nd S-C residue). Compared to the dense 1st S-C sample, the 2nd S-C residue was highly porous, as shown in Fig. 2e, f. As sulfur and carbon are insoluble in water, these pores can be

attributed to the dissolved Li_6PS_5Br. The pores in the 2nd S-C residue (corresponding to the original Li_6PS_5Br particles) range in size from 50 to 500 nm and are interconnected, which should ensure effective ion migration pathways within the cathode. This is a key factor for the power performance of all-solid-state lithium batteries, especially in the case of non-ion-conducting active materials such as sulfur. The 2nd S-C residue particles have a typical size smaller than 100 nm, close to that of super P carbon. This drastic reduction in the particle size, compared to that of the 1st S-C, suggests that sulfur at least partially melted again during the second ball milling. Consequently, the large aggregates of the 1st S-C sample were segregated into smaller carbon-based composite particles (<100 nm) by Li_6PS_5Br. Such uniform mixing of composite cathode with nanoscale particles is essential for a full utilization of the active material during cycling, as it maximizes the reactive electrolyte to electrode interface area and minimizes the thickness of poorly conducting Li_2S_n layers through which Li^+ has to migrate to reach unreacted sulfur.

Figure 3 demonstrates the cyclic voltammogram (CV) of S/Li_6PS_5Br/In-Li cell in the voltage range of 1.0 to 3.0 V vs. Li/Li^+ (0.4 to 2.4 V vs. In-Li). As demonstrated by CV measurements in our earlier work [13], argyrodite electrolyte Li_6PS_5Br is electrochemically stable between 0 and 4 V vs. Li/Li^+. Accordingly, all the peaks observed in the voltammogram shown in Fig. 3 belong to the active cathode material of sulfur. In the first cycle, two cathodic peaks around 2.2 and 1.8 V vs. Li/Li^+ could be seen, in line with observations in literature for conventional liquid electrolyte batteries [18, 19]. The cathodic peak around 2.2 V corresponds to the oxidation of elemental sulfur to higher-order polysulfides (Li_2S_n, $n \geq 4$), while the second cathodic peak around 1.8 V, which is broader with a shoulder at about 1.9 V, is attributed to the further reduction of polysulfides to lower-order polysulfides and finally to Li_2S. For the oxidation process, only one peak around 2.6 V vs. Li/Li^+ could be detected. Oxidation of Li_2S to lower-order polysulfides has slower kinetics compared to the subsequent oxidation to S; this will consequently lead to an overlap of the two reversible reaction steps [20]. During the second and third cycle, however, the cathodic peak around 2.2 V disappeared, leaving only one reduction peak shifted to around 1.7 V [21]. Close matching of the further CV cycles to the 2nd cycle indicates the high reversibility of the sulfur composite cathode and thus high cyclability of the battery.

Room temperature cyclic performance of the all-solid-state S/Li_6PS_5Br/In-Li cell was investigated at a current density of 167 mA/g (0.38 mA/cm^2, corresponding to C/10) between 1.0 and 3.0 V vs. Li/Li^+. As shown in Fig. 4a, an initial discharge capacity of 1355 mAh/g (i.e., 3.06 mAh/cm^2) was achieved. With the prolonged cycling, the overpotential considerably decreased, which could be tentatively ascribed to an improved contact profile of the components within the composite cathode. The discharge-charge curves shifted right (toward lower-order lithium polysulfides) on further cycling and stabilized after 40 cycles. Figure 4b demonstrates the variation of capacity and coulombic efficiency with cycling. At the second cycle, the discharge capacity drastically decreases to 1150 mAh/g, probably due to the severe volume change of active material during cycling $S+2Li \leftrightarrow Li_2S$. Over cycles 2–50, the discharge capacity experienced an average fading of 0.13 % per cycle, representing a high capacity retention of 94 % for 49 cycles, leaving a reversible capacity of 1080 mAh/g at the 50th cycle. Coulombic efficiency reached an average value close to 100 % over cycles 2–50, suggesting that there are hardly any side reactions during cycling. It may be noted that the capacity of the battery still undergoes some fading most probably because of the gradual loss of active material due to the cathode volume changes but periodically, the capacity increases again when further volume changes reestablish electrical contact to the temporarily detached cathode material.

Ex situ XRD was conducted on the composite cathode before and after cycling, as shown in Fig. 5. Due to the amorphization of sulfur after the first ball milling, no peaks corresponding to sulfur could be observed for the composite cathode before cycling. Except for one broad peak around 53° attributed to carbon, all the peaks can be assigned to Li_6PS_5Br. After cycling, no obvious change occurred to the XRD pattern, suggesting that the argyrodite structure was stable throughout the cycling. It is noted that our recent studies on all-solid-state batteries using CuS [15] or Cu-Li_2S [13] as cathode and Li_6PS_5Br as electrolyte revealed that Cu^+ can

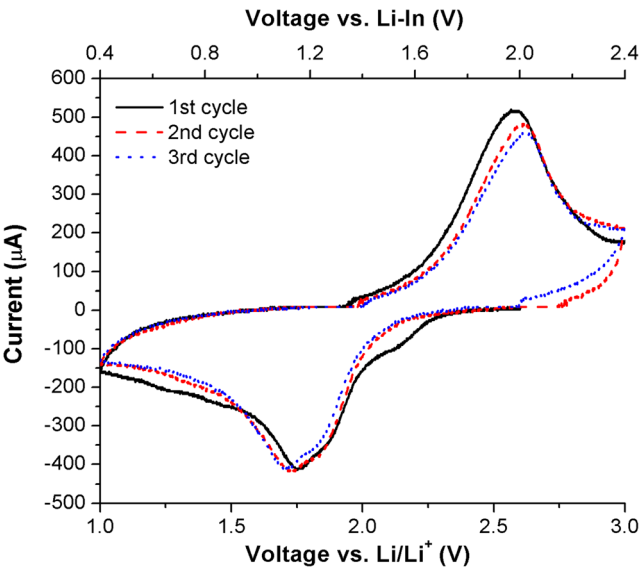

Fig. 3 Cyclic voltammogram of the all-solid-state cell S/Li_6PS_5Br/In-Li in a voltage range of 1.0 to 3.0 V (vs. Li/Li^+) at a scanning rate of 0.02 mV/s. The S content of the composite cathode is 20 wt%. *Top voltage axis* shows the corresponding values of the voltage vs. In-Li

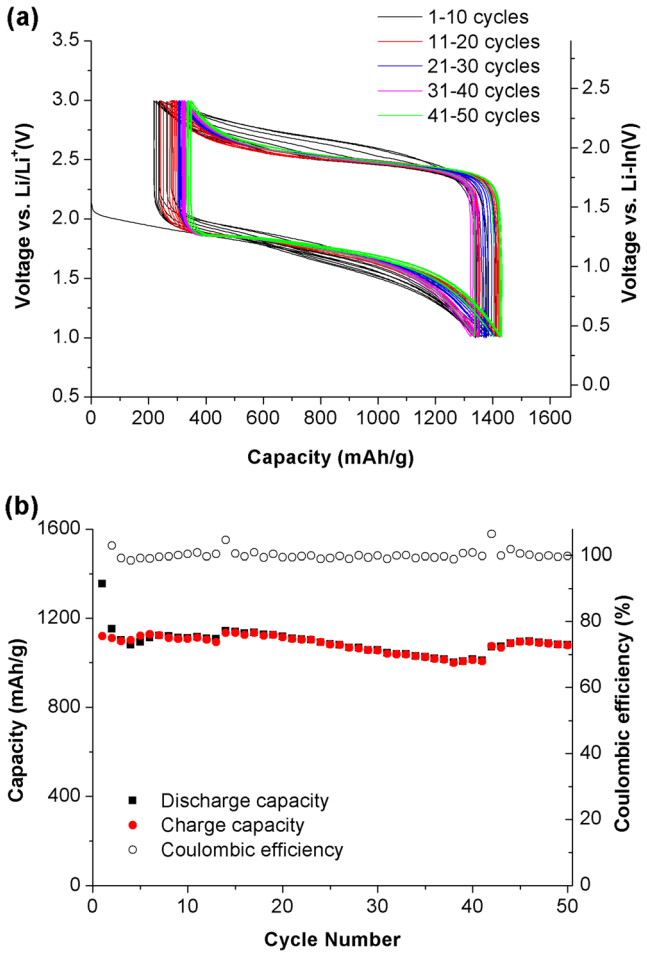

Fig. 4 **a** Discharge-charge curves and **b** discharge/charge capacity and coulombic efficiency of the all-solid-state S/Li_6PS_5Br/In-Li cell up to 50 cycles at room temperature. The current density is 167 mA/g of active sulfur (corresponding to C/10). The voltage range is 1.0 to 3.0 V vs. Li/Li^+. The weight ratio of the components in the composite cathode is S:Li_6PS_5Br:C=20:70:10

be reversibly exchanged for Li^+ in Li_6PS_5Br, leading to mixed mobile ion product $Cu_xLi_{6-x}PS_5Br$. Such complications cannot occur in Li/S batteries so that the favorably high cycling stability of the argyrodite solid electrolyte corroborates its application potential in all-solid-state Li/S secondary batteries.

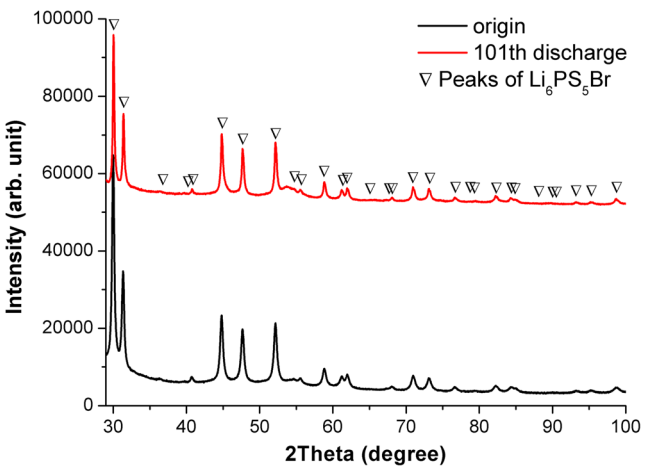

Fig. 5 Ex situ XRD patterns of composite cathode (20 wt% S) before cycling and after 101st cycle (discharged state)

Cyclic performance of all-solid-state Li/S cells using composite cathode with different S content (20, 25, 30, and 40 wt%) were examined. Figure 6 shows the variation of selective discharge capacities with S content of composite cathode (at the 1st, 10th, 15th, and 20th cycles). At the beginning of cycling, a high value of discharge capacity (>1160 mAh/g with respect to the weight of S) was obtained for all the cells, suggesting that most of the sulfur took part into the electrode reaction regardless of the variation of sulfur content. When the S content is 25 wt%, the initial discharge capacity of the cell was 1460 mAh/g of S, which was the highest among all the cells investigated in this study. In Fig. 6, the capacities are shown with respect to the weight of the cathode composite. In this way, the influence of the choice of S content on the energy density of the cell can be read more directly. Only in the 1st cycle, the capacity of the cathode composite rises with the sulfur content. Already after 10 cycles, the discharge capacity at S=25 wt% became the highest as the cells with S contents of 20 and 25 wt% initially showed similarly slow capacity fading, while the capacity of cells with larger S contents faded considerably faster, which could be ascribed to the more severe volume change of the composite cathode due to the higher active material contents. Therefore, in terms of the capacity retention, our cells at 20 and 25 wt% S contents are obviously superior to those with S contents ≥30 wt%. The optimized weight ratio of sulfur in the composite cathode of our cell is therefrom 25 wt%.

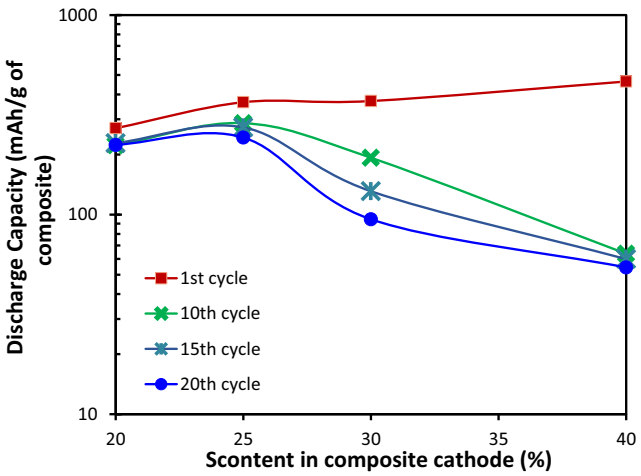

Fig. 6 Discharge capacity of the all-solid-state cells using composite cathode mixture with various S contents, i.e., 20, 25, 30, and 40 wt%. Here, the discharge capacity is given with respect to the total weight of the composite cathode as a more direct measure for the energy density of cells based on these composites. Discharge capacity curves are shown only for the 1st, 10th, 15th, and 20th cycle for clarity

Conclusions

Sulfur composite cathodes were prepared by two-step ball milling, leading to amorphous sulfur incorporated in super P carbon with a particle size smaller than 100 nm. Reducing the particle size of the active materials benefits cycling performance of the battery. The resulting all-solid-state Li/S battery using Li_6PS_5Br as the solid electrolyte showed an initial discharge capacity of 1355 mAh/g and reversible capacity of 1080 mAh/g after 50 cycles. Increasing the sulfur content in the composite cathode enhances the initial discharge capacity (per gram of composite mixture) nearly proportional to the S content but the reversible capacity is significantly higher for cells with low S contents, emphasizing the decisive role of the volume changes of the active material in the capacity fading. To improve the capacity retention of Li/S batteries, we therefore plan to further enhance the strain buffering effect of the carbon component.

Acknowledgments This research was supported by the National Research Foundation, Prime Minister's Office, Singapore under its Competitive Research Programme (CRP Awards No. NRF-CRP 8-2011-4 and NRF-CRP 10-2012-6).

References

1. Barghamadi M, Kapoor A, Wen C (2013) J Electrochem Soc 160: A1256–A1263
2. Gao J, Lowe MA, Kiya Y, Abruña HD (2011) J Phys Chem C 115: 25132–25137
3. Xiong S, Kai X, Hong X, Diao Y (2011) Ionics 18:249–254
4. Kobayashi T, Imade Y, Shishihara D, Homma K, Nagao M, Watanabe R, Yoboi T, Yamade A, Kanno R, Tatsumi T (2008) J Power Sources 182:621–625
5. Nagao M, Hayashi A, Tatsumisago M (2011) Electrochim Acta 56: 6055–6059
6. Nagao M, Hayashi A, Tatsumisago M (2013) Energy Technol 1:186–192
7. Agostini M, Aihara Y, Yamada T, Scrosati B, Hassoun J (2013) Solid State Ionics 244:48–51
8. Lin Z, Liu Z, Fu W, Dudney NJ, Liang C (2013) Angew Chem Int Ed 52:7460–7463
9. Deiseroth HJ, Kong ST, Eckert H, Vannahme J, Reiner C, Zaiß T, Schlosser M (2008) Angew Chem Int Ed 47:755–758
10. Rao RP, Adams S (2011) Phys Status Solidi A 208:1804–1807
11. Rayavarapu PR, Sharma N, Peterson VK, Adams S (2011) J Solid State Electrochem 16:1807–1813
12. Prasada Rao R, Sharma N, Peterson VK, Adams S (2013) Solid State Ionics 230:72–76
13. Chen M, Rao RP, Adams S (2014) Solid State Ionics 262:183–187
14. Stadler F, Fietzek C (2010) ECS Trans 25:177–183
15. Chen M, Rao RP, Adams S (2014) Solid State Ionics. doi:10.1016/j.ssi.2014.05.004
16. Ji X, Lee KT, Nazar LF (2009) Nat Mater 8:500–506
17. Simmonds AG, Griebel JJ, Park J, Kim KR, Chuang WJ, Oleshko VP, Kim J, Kim ET, Glass RS, Soles CL, Sung YE, Char K, Pyun J (2014) ACS Macro Lett 3:229–232
18. Zhou X, Xie J, Yang J, Zou Y, Tang J, Wang S, Ma L, Liao Q (2013) J Power Sources 243:993–1000
19. Zhang B, Qin X, Li GR, Gao XP (2010) Energy Environ Sci 3:1531–1537
20. Li K, Wang B, Su D, Park J, Ahn H, Wang G (2012) J Power Sources 202:389–393
21. Zhang B, Lai C, Zhou Z, Gao XP (2009) Electrochim Acta 54:3708–3713